COMMUNICATIONS IN
SCIENCE AND TECHNOLOGY
Homepage: cst.kipmi.or.id

Insight into aluminum leaching with microwave from peat clay: A comparative kinetic study of SC and BIC models

Agus Mirwan[a], Hairullah[a], Rinny Jelita[a], Jefriadi[a], Meilana Dharma Putra[a,*],Bintang Hambela Ilmanto[a], Hexas Sarastiwi Handayani Putri[a], Muhammad Bahrul Ulum[a], Muhammad Rofi Haka[a], Muhammad Arif Darmawan[b]

[a]*Department of Chemical Engineering, Lambung Mangkurat University, Banjarbaru 70714, Indonesia*
[b]*Research Center for Industrial Process and Manufacturing Technology, Research Organization for Energy and Manufacture, National Research and Innovation Agency, Jakarta Pusat 10340, Indonesia*

Article history:
Received: 30 November 2025 / Received in revised form: 19 December 2025 / Accepted: 21 December 2025

Abstract

The depletion of bauxite reserves has prompted the research of various types of soil as alternative sources of aluminum, such as the peat clay used in this study. The complexity of the minerals requires a more efficient leaching methods, while microwave-based leaching offers a potential approach through rapid and uniform heating. This study examines the effect of microwave power, HCl concentration, operating temperature, and particle size on the leaching efficiency of aluminum from peat clay soil. The leaching process was modeled using two approaches, namely the shrinking core (SC) model and the broken-intact cell (BIC) model under pseudo-steady state conditions. The results showed that increasing HCl concentration, microwave power, and temperature accelerated leaching, while increasing particle size decreased leaching efficiency. Optimum conditions were achieved at 4 M HCl concentration, 100 W power, 40 °C temperature, and 0.0074 cm particle size. The shrinking core (SC) model showed better fit under most conditions, while the intact-broken cell (BIC) model was more accurate at lower temperatures and particle sizes. The simulation results showed that the most suitable parameter values in the SC model were De = 0.0049 cm²/s, k = 10.5 cm/s, and kc = 2.49 cm/s, while in the BIC model De = 0.04808 cm²/s and K = 0.02689 g/cm³ were obtained. These results confirm the superiority of the SC model in representing microwave-based leaching mechanisms in general, while the BIC model provides additional insights under diffusion-limited conditions. Process Performance Index (PPI) analysis showed that optimum conditions were achieved at 4 M HCl and 40 °C, but lower acid concentrations also yielded competitive PPI. This confirms that leaching effectiveness is determined by a combination of alumina recovery and reagent consumption efficiency. These findings contribute to the development of leaching kinetics models and the optimization of more efficient and energy-saving aluminum extraction processes.

Keywords: Microwave-assisted leaching; aluminum; shrinking core; peat clay; broken and intact cells; kinetic model

1. Introduction

Aluminum is a strategic metal that is widely used in various industrial sectors such as transportation, construction, and energy [1]. Until now, the main source of aluminum has come from bauxite, but its reserves are increasingly limited and the mining process has a major impact on the environment [2]. This condition has encouraged the search for alternative sources of aluminum from non-bauxite mineral materials that are abundant in nature, including various types of clay and mineral residues [3].

One potential material is peat clay, which is a layer of clay that is at a depth of around 1.5–3.0 meters below the surface of the peat soil. Peat soil, known as peatlands, is spread evenly across various countries in some parts of world such as North America, Europe, Southeast Asia, Africa, South America [4–7]. It was reported [2] that peat clay soils have high mineral content of silicon oxide (SiO_2), calcium oxide, iron oxide (Fe_2O_3), titanium oxide (TiO_2), aluminum oxide (Al_2O_3), calcium oxide

* Corresponding author.
Email: mdputra@ulm.ac.id
https://doi.org/10.21924/cst.10.2.2025.1850

(CaO), and other oxide contents detected at relatively low levels. Peat clay contains approximately 7.20% Al_2O_3, which can be increased to 17.90% through calcination. This compound has the potential to be used as a catalyst, coagulant, and adsorbent in water treatment processes [4,8]. Therefore, efforts to improve the leaching process of aluminum oxide from peat clay soil are worthy of being a focus for related industries, considering the very diverse potential uses of this material.

Various leaching methods have been applied to extract aluminum from mineral-rich materials, including alkaline leaching using NaOH or KOH and organic leaching using citric acid or deep eutectic solvents [9–11]. However, alkaline leaching generally requires high temperatures and produces a passive silicate layer that reduces efficiency, while organic leaching has a slow reaction rate and requires expensive reagents [12]. Compared to these methods, acid leaching - especially with HCl- is recommended because it provides high reactivity toward Al_2O_3, is selective toward impurities, and allows efficient solvent regeneration [13,14].

Wang et al. [15], perform the acid leaching method of vanadium from black shale by microwave-assisted heating and provide higher leaching results compared to conventional heating. The MAL (Microwave-Assisted Leaching) technique is used to accelerate and improve the leaching process of various mineral materials and secondary resources, especially copper ore, nickel ore, waste sludge, fly ash, and industrial dust [16]. Compared to conventional methods, MAL has several prominent advantages, especially in its application in the fields of hydrometallurgy, food industry, pharmacology, and natural ingredient-based therapy [17–19]. The technique of leaching aluminum from peat clay using acid with the help of microwaves is considered prospective in the field of MAL because it can shorten processing time, increase the recovery percentage, and is more environmentally friendly. Although the maintenance costs of microwave equipment are higher [20,21], this method saves energy up to one-tenth of the conventional process and increases selectivity so that energy and solvent use can be reduced [22].

To understand and optimize the leaching process, kinetic modeling is required that can accurately describe the mass transfer and reaction mechanisms. Mathematical modeling in engineering allows for control simplification, process optimization and design, and provides accurate data for equipment scale-up. Furthermore, kinetic laws provide a clearer understanding of leaching behavior [23]. The proposed mathematical approach is developed through the integration of differential equilibrium mass balances, focusing on macroscale mass transfer mechanisms. The shrinking core (SC) model can predict that the reaction process begins at the outer surface of the particle and then progresses to the inner unreacted zone. The reaction layer is depicted as an ash layer, assumed to be unreacted.

The macroscopic shrinking core model approach has been used for solid–liquid reactions under conventional heating and has been successfully applied to aluminum leaching data from water treatment sludge and peat clay [14]. Aluminum leaching has been modeled using the SC model in our previous study, but its application was limited to specific temperature conditions. The SC model assumes that aluminum resides in the solid core of peat particles that shrink during extraction, follows first-order kinetics, and reaches linear equilibrium at the solid–liquid interface, with the effective diffusivity, mass transfer coefficient, and reaction rate constant as the main variables.

In addition to SC, the Broken and Intact Cell (BIC) model introduced by Sovová [24], offers the ability to explain leaching rates in two extraction phases—fast and slow—by considering the presence of broken and intact cells within the particles. The BIC model is able to describe the slope of the extraction curve at the initial and later stages separately, as well as the transition to slower extraction due to cell wall damage by grinding. Particles are assumed to consist of two zones, namely damaged cells and intact cells, each containing solute [24]. Solutes within broken cells readily dissolve due to the cell walls being destroyed by grinding, while those within intact cells dissolve more slowly [25]. Macroscale BIC modeling was first applied by Bucić-Kojić et al. [26] to the extraction of phenolic compounds from grape seeds, using effective diffusivity and partition constants as fitting parameters. Most subsequent studies have also used the BIC model for the leaching of organic compounds from plants, but it has not been widely applied to mineral materials.

Based on this, this study evaluates microwave-assisted aluminum leaching from peat clay soil with variations in microwave power, acid concentration, temperature, and particle size. The novelty of this study lies in the application of the BIC model and the utilization of the SC model in conjunction with BIC to describe the kinetic behavior of aluminum leaching more comprehensively based on the experimental results.

2. Material and Methods

2.1. Leaching process

Peat clays sourced from local area in Banjarbaru, South Kalimantan, Indonesia are cleaned of small logs and other impurities. Then drying is conducted in direct sunlight. After going through a grinding and sieving process to achieve particle sizes of 0.0074 and 0.0149 cm, the samples were then calcined at 700 °C for 120 minutes. Peat clay samples were calcined at 700 °C to promote dehydroxylation of aluminosilicate clay minerals, specifically the transformation of kaolinite to metakaolin. This temperature was chosen because it is above the generally reported dehydroxylation range for kaolinite (±450–650 °C), thus achieving an effective dehydroxylation rate without triggering the formation of spinel or mullite phases, which are less reactive to acid leaching. Calcination was performed as a pretreatment step to increase the reactivity of the solids to the leaching process.

The apparatus for microwave-assisted leaching was first assembled as shown in Fig. 1. Then, 5 grams of sieved peat soil together with 1 M HCl solution were put into a three-necked flask. Then the power in the microwave is set at 100 W and the

operating time is set for 60 minutes. The stirring motor is turned on and the speed is 300 rpm. Then, the sample solution was drawn using a syringe periodically at 5, 10, 15, 20, 25, 30, 40, 50, and 60 minutes. Then the sample was collected in a sample flask. The process of leaching was reiterated for 2 and 4 M HCl solution at 80 W power and temperatures of 25, 30, and 40 °C. Analysis was carried out on peat clay soil both before and after calcination using analytical methods SEM-EDX, FTIR, XRD, and XRF. SEM-EDX analysis was used to identify the morphology of peat clay and elemental composition through SEM analysis type EVO MA 10 integrated with an energy-dispersive detector. The characteristic properties of compounds in peat soil of each functional group were identified through FTIR analysis. This analysis uses the Shimadzu Model with a band span of 500-4000 cm^{-1} and transmission in percent (%). The XRD patterns of peat clay were obtained using a Philips X-pert powder diffractometer, and the mineralogical composition was qualitatively searched and matched against the PDF-2 (1996) database using X'Pert HighScore Plus software. XRF analysis uses PANalytical miniPAL 4 type which aims to determine the chemical composition of minerals quantitatively. The aluminum content in Samples was analyzed using Inductively Coupled Plasma-Optical Emission Spectroscopy (ICP-OES) (9060-D Teledyne Leeman Labs, USA) with three repetitions to obtain the average. Prior to analysis, the solution was separated from the solid residue by filtration and then diluted with ultrapure water until it was within the instrument's working concentration range. The sample was then acidified using concentrated HNO_3 to a pH <2 to stabilize the metal ions and prevent precipitation before measurement. ICP-OES calibration was performed using a multi-point aluminum standard solution, and all measurements were carried out according to the instrument's standard operating procedures.

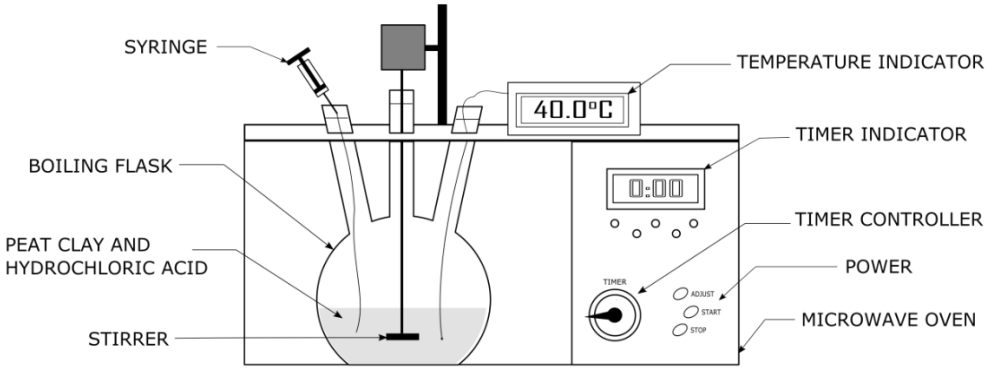

Fig. 1. Microwave-assisted leaching devices

2.2. Shrinking core (SC) model

To obtain a shrinking core model, several assumptions need to be made, among which peat clay soil is assumed to have spherical particles and no decrease in temperature during the process. Compounds other than aluminum present in peat clay soil are assumed to have no significant effect on the process kinetics. Particles are considered to be homogeneous and maintain their spherical shape, although in certain cases they may have an effect. Based on the regard that leaching occurs in a stirred reactor system, the mass balance equation is formulated as follows:

Total mass balance equation for the leaching process:

$$\frac{dC_{Al}}{dt} = \frac{k_c}{R}\frac{(1-\varepsilon)}{\varepsilon}\left(C_{A(R)} - C_{Al}\right) \quad (1)$$

Changes in the concentration of aluminum as a dissolved substance in the solid phase (peat clay) are influenced or related to its mass transfer coefficient:

$$\frac{\overline{dq}}{dt} = \frac{4\pi R^2 k_c \rho_p}{3m}\left(C_{A(R)} - C_{Al}\right) \quad (2)$$

Diffusion equation outside the particle:

$$-\frac{d}{dr}\left(-D_e 4\pi r^2 \frac{dC_{A(R)}}{dr}\right) = 0 \quad (3)$$

Equation (4) contains the initial conditions and Equations (5) to (6) contain the boundary conditions which are detailed as follows:

$$r_c = R \text{ and } \bar{q} = q_u \text{ at } t = 0 \quad (4)$$

$$r = r_c \rightarrow D_e \frac{dC_{A(R)}}{dr} = kC_{A(R)} \quad (5)$$

$$-D_e \frac{dC_{A(R)}}{dr} = k_c\left(C_{A(R)} - C_{Al}\right) \quad (6)$$

The average concentration of dissolved substances in the solid phase:

$$\frac{\bar{q}}{q_u} = \left(\frac{r_c}{R}\right)^3 \quad (7)$$

The integration of Equation (3) produces an equation (8):

$$C_{A(R)} = -\frac{K_1}{r} + K_2 \tag{8}$$

While the equation (5) was substituted into the equation (8), the equation (9) was obtained:

$$K_1 = \frac{kK_2 {r_c}^2}{\left(D_e + kr_c\right)} \tag{9}$$

The equation (10) was obtained when equation (8) was substituted into the equation (6):

$$K_2 = \frac{k_c C_{Al}\left(D_e + kr_c\right)R^2}{D_e\left(k{r_c}^2 + R^2 k_c\right) + k_c k\left(r_c R^2 - {r_c}^2 R\right)} \tag{10}$$

Equation (10) is inserted into the equation (9); then, these two equations are also substituted into the equation (8) hence obtaining equation (11):

$$C_{A(R)} = \frac{kk_c C_{Al} R^2 {r_c}^2 + k_c C_{Al}\left(D_e + kr_c\right)R^2}{D_e\left(k{r_c}^2 + R^2 k_c\right) + k_c k\left(r_c R^2 - {r_c}^2 R\right)} \tag{11}$$

2.3. Broken and intact cells (BIC) model

The BIC model was adopted from the Bucić-Kojić et al. [26]. The BIC model in the stirred leaching process was developed using several assumptions:

- The leaching process is in the first order reaction by illustrating that the crushed particles have broken cells and intact cells.
- In calculating the level of dissolved substances in the solid phase before extraction, it is assumed that a particle is thought to have cells or cavities where solutes are stored. When the particles of a material are crushed, the cell walls in the area near the surface of the particles are damaged and the solutes from these cells are then easily dissolved in the solvent.
- The equilibrium was initially assumed to occur between the open cell region and the liquid phase, as an effort to simplify the calculation, the resistance of mass transfer in damaged cells and the process parameters in the form of a stirred liquid were ignored.

The mass balance equation of the solute in the liquid phase:

$$c_{Al} = \frac{q_u - \left(1-f\right)q_i}{\left(f/K\right) + B} \tag{12}$$

Changes in the concentration of aluminum as a dissolved substance in the solid phase (peat clay) of intact and broken cells are related to the rate of mass transfer of the solute:

$$\frac{dq_i}{dt} = -\frac{M}{m\left(1-f\right)} \tag{13}$$

$$\left(1-f\right)q_i + f\frac{c_{Al}}{K} + Bc_{Al} = q_u \tag{14}$$

Where the first part deals with intact cells, the second part with fractions c_{Al}/K associated with broken cells. The third part is related to the liquid phase. The speed of mass transfer through the entire surface of the particle core A_i:

$$M = k_p A_i \rho_p \left(q_i - \frac{c_{Al}}{K}\right) \tag{15}$$

Initial condition for solute at untreated material:

$$q_i = q_u \text{ at } t = 0 \tag{16}$$

Equations that show the relationship between volumetric fractions with particle radius (17), relationship of volumetric fractions with surface area of particles (18), and the relationship of mass transfer coefficient with effective diffusivity and particle radius (19):

$$f = \left(\frac{R_i}{R}\right)^3 \tag{17}$$

$$f^{\frac{2}{3}} = \frac{A_i}{A} \tag{18}$$

$$k_p = \frac{5D_e}{R} \tag{19}$$

Equation (13) integrated, equation (15) substituted into the equation (13) and c_{Al} eliminated using the equation (14) so that the equation is obtained (20):

$$q_i = \frac{q_u}{1+BK}\left\{1 + BK.\exp\left[-\frac{k_p A_i \rho_p}{m\left(1-f\right)}\frac{1+BK}{BK+f}t\right]\right\} \tag{20}$$

Recovery is a comparison between the reduction of a solute in the solid phase and the solute initially given as:

$$recovery = \frac{q_u - q(t)}{q_u} \times 100\% \tag{21}$$

Differential equation (13) combined with the equation (15) solved using programming computing GNU Octave software. Leaching curves are described as recovery versus time. While processing graphics using SciDAVis software.

2.4. Process performance index (PPI)

The basis of process performance index (PPI) is roughly evaluated based on the process implemented in industrial scale (50 L HCl and 5 kg peat clay).

$$m_{Al} = m_0 \times (\eta / 100) \quad (22)$$

where m_{Al} is the Al recovered, m_0 is the alumina content in peat clay amount per batch in industrial scale and η is present of Al recovery. This equation provides the actual output value of the process (output), and is the main component in determining the net process value.

The revenue of Al is evaluated using the following equation:

$$R = m_{Al} \text{ x } P_{Al} \quad (23)$$

R is the revenue of the obtained Al, while the P_{Al} is the price of alumina (about $0.0025/g). This revenue is not intended for commercial profit analysis, but rather as a numerical proxy for assessing extraction yield in universal units so that it can be compared proportionally with operational costs.

Process energy is calculated by considering a 20-minute heating duration and effective microwave power (half the nominal power, as microwaves operate on a duty cycle modulation basis). Industrial-scale energy is assumed to be 10 times that of laboratory-scale energy:

$$E = P_{\text{real}} \times 1200 \quad (24)$$

$$C_E = \left(\frac{E}{3{,}600{,}000}\right) \times 0.01 \quad (25)$$

With an energy tariff of USD 0.01/kWh, energy costs are negligible and contribute only a minor portion to the total process cost.

Industrial-scale HCl solutions are reused repeatedly through a chemical regeneration process. Therefore, only a small portion of the solution needs to be replaced each cycle (make-up). This study used a conservative assumption of 1% make-up:

$$C_{HCl} = 0.01 \text{ x } C_{full} \quad (26)$$

This 1% make-up approach is commonly used in industrial hydrometallurgical processes, where HCl regeneration can take tens to hundreds of cycles. Thus, the contribution of HCl cost to the total process cost is very small, making the evaluation more focused on technical aspects such as extraction efficiency and operating conditions. Operating costs are calculated by adding energy costs and HCl make-up costs:

$$\boldsymbol{C}_{\text{tot}} = \boldsymbol{C}_{\boldsymbol{E}} + \boldsymbol{C}_{\text{HCl}} \quad (27)$$

This value represents the operational capital required to run the process per batch on an industrial scale.

To assess the effectiveness of each condition, the following index is used:

$$\text{PPI} = \frac{R}{C_{\text{tot}}} \quad (28)$$

A high PPI indicates a highly efficient process, as the output value is significantly greater than the input value. A low PPI indicates a less effective process, although it can still be positive. The PPI is not a measure of commercial profitability, but rather a technical indicator that shows the ratio of process effectiveness to resource expenditure. Therefore, the PPI is well-suited for optimizing low-energy leaching processes and acid regeneration.

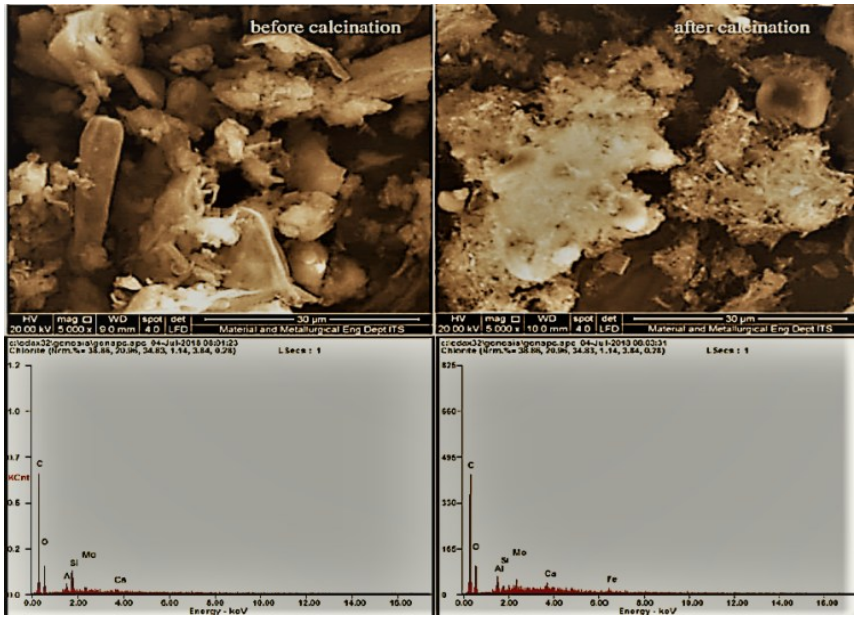

Fig. 2. Results of SEM-EDX analysis of peat clay soils before and after calcination

3. Results and Discussions

3.1. SEM-EDX characterization

In this study, the effect of microwave power, HCl concentration, temperature, and particle size of peat clay soil on aluminum recovery from peat clay soil was studied by comparing experimental and modeling results. The surface morphology of peat clay before and after calcination was analyzed using SEM-EDX as shown in Fig. 2. The analysis results showed that the clay surface before calcination still showed an irregular aggregate structure with low porosity, while after calcination the surface appeared more porous and experienced recrystallization due to the release of structural water and dehydroxylation.

EDX analysis confirmed that the dominant elements were Si, Al, and Fe with compositions of 2.31%, 5.48%, and 2.63% by weight before calcination, respectively, and increased to 3.07%, 1.72%, and 3.94% by weight after calcination. The increase in Al and Fe content and changes in the proportion of Si indicate the relative concentration of elements due to the loss of volatile components such as water and organic carbon. Mineralogically, the main components consist of aluminosilicates (kaolinite, $Al_2Si_2O_5(OH)_4$), quartz (SiO_2), and iron minerals such as nontronite [4,27]. These morphological and compositional changes indicate that the calcination process improves pore openness and increases surface reactivity, thus potentially increasing the efficiency of aluminum leaching in the next stage.

3.2. FTIR characterization

FTIR characterization was used to identify functional groups and variations in mineral structure in peat clay soil samples, as shown in Fig. 3. FTIR spectra were recorded in the 4000–500 cm^{-1} range. The main absorption bands indicate the presence of quartz, kaolinite, illite, and calcite with the vibration variations of -OH, Si-O and Al-O bonds. The presence of quartz is marked by vibration stretching Si-O carried on 421, 994, and 1099 cm^{-1} for peaks after calcination. Presence of kaolinite is mostly shown in arcs 548, 694, 753, 1099, and 3445 cm^{-1} after calcination. Illite composition is indicated by warping 753, 1640, and 3445 cm^{-1} after calcination, while the presence of calcite compounds is shown in arcs 1640 cm^{-1} after calcination [28]. The low transmittance band at 910 – 730 cm^{-1} is ascribed to Si-O and Si-O-Si(Al) vibration stretching of illite, while transmittance band at 730 – 420 cm^{-1} assigned to Si-O-Al stretching and Si-O bending of illite [29].

The FTIR spectra show major absorption bands at approximately 3445 cm^{-1} and 1640 cm^{-1}, which are generally associated with –OH stretching and H–O–H bending of adsorbed water and hydroxyl groups in clay minerals. These bands are not interpreted as exclusive indicators of the presence of kaolinite or calcite, but rather reflect the presence of hydroxyl groups and residual moisture still bound to the aluminosilicate structure. Therefore, FTIR results are used as an indication of changes in the –OH group environment during thermal treatment and leaching, not as a sole determinant of specific mineral phase transformations.

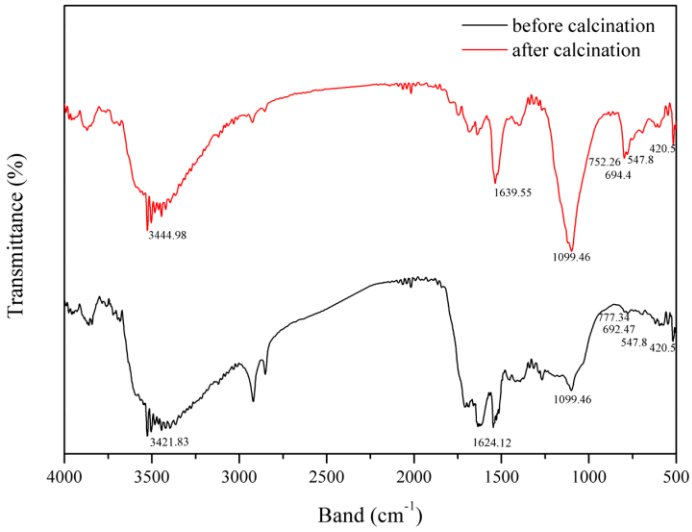

Fig. 3. FTIR spectrum of peat soil before and after calcination

3.3. XRD characterization

The chemical composition and crystal structure of peat clay before and after calcination were analyzed using XRD as shown in Fig. 4 with a diffraction angle range of 2θ in the range of 5°-60°. Based on the PDF-2 database (1996), the characteristic peaks indicate the presence of kaolinite (Ref. 00-001-0527), albite (Ref. 00-001-0739), sillimanite (Ref. 00-001-0614; 00-001-0626; 00-001-0627), and montmorillonite (Ref. 00-002-0009). The dominant compounds observed are kaolinite (aluminum silicate hydrate) and albite (sodium aluminum silicate hydrate) [4,27].

Before calcination, the XRD pattern shows relatively broad and less sharp peaks, indicating a crystal structure that is still irregular and contains organic amorphous components. After calcination, the main peaks in kaolinite and albite become sharper and their intensity increases, indicating increased crystallinity and the loss of the amorphous organic fraction due to thermal decomposition. New peaks at approximately 2θ = 26°–28° and 31°–33° indicate the formation of a sillimanite phase and the partial transformation of kaolinite into amorphous metakaolinite, consistent with the FTIR results showing the loss of –OH groups due to dehydroxylation. Montmorillonite was also identified with lower intensity, indicating that its structure partially collapsed due to heating. In general, peat clay soils are dominated by quartz, hematite, kaolinite, and montmorillonite, with minor mineral variations depending on the geological setting. This is consistent with the report by Cao et al. [30] on peat soils from Lake Dianchi, China, which showed a dominance of silica and orthoclase, and research in Johor, Malaysia, which identified pargasite, dellaventuraite, and richterite [31]. These differences are caused by variations in the geochemical environment and sources of peat-forming materials at each location.

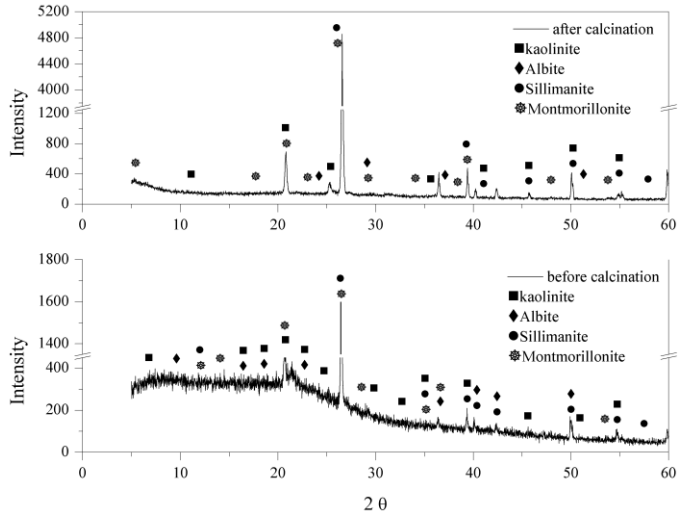

Fig. 4. XRD characterization on peat clay before and after calcination

The XRD analysis results indicate changes in the relative intensity and the appearance or attenuation of diffraction peaks after calcination and leaching. These changes are interpreted as an indication of structural transformation, including the formation of metakaolin phases which are generally characterized by reduced crystal regularity and increased amorphous fraction at temperatures above 500–600 °C. Therefore, XRD in this study was used for phase identification and qualitative evaluation of mineral transformations, and was not intended to conclude an increase in absolute crystallinity because no quantitative crystallinity index was calculated.

On the other hand, the indication of dehydroxylation due to calcination at 700 °C is qualitatively supported by the FTIR and XRD results, which show a weakening or disappearance of the typical kaolinite peaks and a reduction in the structural –OH bands. Although TGA/DTG analysis was not performed to quantitatively verify the mass loss, these changes in structural characteristics are widely used in the literature as indicators of metakaolin formation. Therefore, these characterization results are considered sufficient to support the purpose of calcination pretreatment in the context of this study.

3.4. XRF analysis

Table 1 shows the chemical composition of post-burning peat clay soil using XRF analysis. In general, peat clay soil is dominated by the oxide compounds SiO_2 (31.90%), Al_2O_3 (17.90%), Fe_2O_3 (11.40%), CaO (14.70%), and TiO_2 (8.72%), while other oxides such as K_2O, Cr_2O_3, MnO, NiO, CuO, and P_2O_5 are present only in small amounts. The high SiO_2 and Al_2O_3 contents indicate that peat clay soil has potential as an alternative source of aluminum and active aluminosilicate-based materials. The presence of significant amounts of CaO and Fe_2O_3 also suggests their possible contribution to the surface reactivity and adsorptive capacity of the material after calcination. These results are consistent with previous study [1,32], which reported that the dominant oxide compounds in peat soil are SiO_2, Fe_2O_3, Al_2O_3, and TiO_2 with minor amounts of other oxides, as observed in West Sumatra peat soil where the Si, Al, Fe, and Ca contents reached 50.52%, 13.54%, 12.23%, and 4.98%, respectively. This dominant oxide composition is in line with the XRD and FTIR results which showed the presence of quartz, kaolinite, and illite minerals as the main phases after calcination.

Table 1. Chemical composition of peat soils after calcination

Compound	Content (%)
SiO_2	31.90
Fe_2O_3	11.40
Al_2O_3	17.90
K_2O	0.76
CaO	14.70
TiO_2	8.72
V_2O_5	0.25
Cr_2O_3	1.57
MnO	0.17
NiO	0.091
CuO	0.17
P_2O_5	0.86

It should be emphasized that the aluminum content used as representative data in the leaching analysis and kinetic modeling in this study was determined using ICP-OES. This technique provides a reliable quantitative measurement of the dissolved Al concentration in the liquid phase, making it relevant for evaluating leaching efficiency and determining kinetic parameters. In contrast, XRF is used to describe the total elemental composition of the solids in bulk, while SEM-EDX is semi-quantitative and local, primarily utilized for morphological analysis and elemental distribution on surfaces. Therefore, differences in Al values between methods reflect differences in measurement basis and analytical objectives, and are not intended to be directly compared.

3.5. Mechanism of leaching

SEM-EDX, FTIR, XRD, and XRF characterization results indicate that peat clay contains the main minerals kaolinite, illite, montmorillonite, and quartz, which are rich in aluminum, silicon, and iron. These minerals are chemically stable in aluminosilicate (Al–O–Si) bonds, requiring aggressive leaching conditions to release Al^{3+} ions into solution [33,34]. The process of leaching metals from mineral materials using strong acids such as HCl essentially involves two main stages: (1) diffusion of H^+ ions from the solution to the surface of the solid particles (external diffusion film), and (2) a chemical reaction between H^+ and metal oxide groups (Me–O–Me or Me–O–Si) on the particle surface [35,36].

In clay minerals such as kaolinite, montmorillonite, and illite, which contain aluminum in the form of Al–O–Si or Al–OH–Si, the H^+ ion from HCl acts as an active proton that breaks the Al–O bond through a protonation reaction, producing dissolved aluminum ions (Al^{3+}) or $AlCl_n^{3-}{}_n$ complexes in solution [37,38]. The main reaction can be written as:

$$\text{Al–O–Si} + 6H^+ \rightarrow \text{Al}^{3+} + \text{Si(OH)}_4 \quad (22)$$

$$\text{Al}_2\text{O}_3 + 6HCl \rightarrow 2\text{AlCl}_3 + 3H_2\text{O} \quad (23)$$

Thus, H^+ ion transfer (proton diffusion) is a key step determining the aluminum leaching rate, especially in the early stages of the process. Under certain conditions, the leaching rate can be controlled by external diffusion (a liquid film surrounding the particle) or surface chemical reactions, depending on particle size, acid strength, and microwave energy intensity used [39]. The understanding of this proton transfer mechanism is crucial to explaining the variation in leaching behavior across process parameters such as temperature, microwave power, and HCl concentration, which will be discussed in the next section.

3.6. Effect of microwave power

The effect of microwave power (80 and 100 Watt) on aluminum recovery by comparing two calculation models at particle size of 0.0074 cm and 1 M HCl concentration was shown in Fig. 5. In general, increasing microwave power accelerates the leaching rate and increases the aluminum recovery percentage. Increasing the power increases thermal agitation in the liquid-solid system, thereby reducing diffusion barriers and accelerating the leaching reaction. Modeling results (Table 2) show that in the Shrinking Core (SC) model, increasing the power from 80 W to 100 W causes a decrease in the effective diffusivity (De) from 0.002708 to 0.001390 cm²/s, but is accompanied by a significant increase in the reaction rate constant (k) from 1.28 to 3.58 cm/s. This indicates that the dominant effect of high power is an increase in the chemical reaction rate at the solid-liquid interface. In contrast, in the Broken and Intact Cell (BIC) model, De and K values increased with increasing power (from De = 0.0508 to 0.08039 cm²/s; from K = 0.0102 to 0.0106 g/cm³), indicating more efficient diffusion due to increased microthermal agitation. On the other hand, as microwave power increases, the mass transfer coefficient decreases while the reaction rate increases. Meanwhile, the decrease in the mass transfer coefficient is accompanied by an increase in the mass transfer resistance. This is reasonable, because in liquid-solid systems, mass transfer resistance is an important factor that affects the efficiency of solute movement from the liquid phase to the solid phase [40]. Furthermore, this resistance is inversely proportional to the mass transfer coefficient; as the mass transfer coefficient decreases, the resistance increases, thus inhibiting the ability of the solvent to penetrate and interact with the solid particles effectively [40–42]. Overall, these results confirm that increasing microwave power has a dual effect: accelerating leaching kinetics by increasing reaction energy, but also increasing diffusion resistance under certain conditions [43–45]. The SC model showed the best fit to the experimental data with a slightly lower RMSE value than the BIC model, indicating that the leaching process at this power was driven more by chemical reactions than by internal diffusion. Furthermore, higher power increases thermal agitation and accelerates the leaching reaction by reducing the diffusion resistance in the particles [46]. However, at higher powers, excessive thermal effects could potentially cause inhomogeneity in the heat distribution and reduce mass transfer efficiency [47].

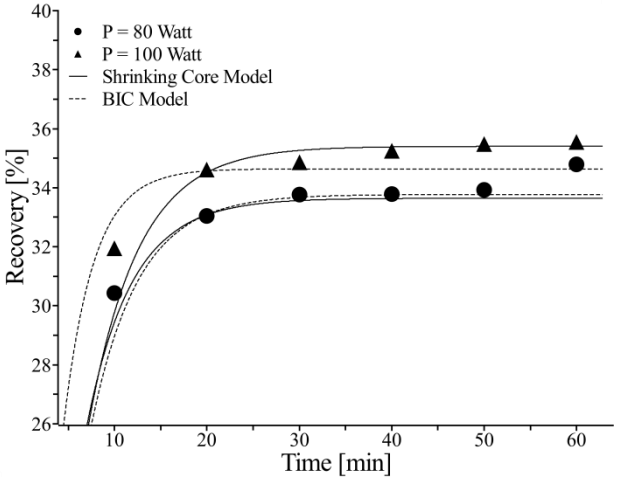

Fig. 5. Recovery of aluminum at varying microwave power (80 and 100 W): comparison of two calculation models on 0.0074 cm particles with 1 M HCl

The effective diffusivity (De) values obtained from the Shrinking Core model in this study are pseudo-parameters representing the overall internal diffusion resistance, rather than intrinsic molecular diffusivity. Although increasing microwave power is generally reported to enhance diffusion in various leaching systems, results obtained on calcined peat clays show a different response. At higher microwave powers (80–100 W), rapid volumetric heating can potentially cause changes in the microstructure of the solid, including pore restructuring and the formation of denser reaction product layers, thereby increasing the internal diffusion resistance within the Shrinking Core model framework. Consequently, the De values extracted from the model appear to decrease pseudo-parameterically, reflecting the model's limitations in capturing microwave-induced internal structural changes, rather than indicating an increase in diffusion processes.

3.7. Effect of HCl concentration

The effect of HCl concentration (1, 2, and 4 M) on the recovery rate of the leaching process for both models on 100 Watt of microwave power and 0.0074 cm particle size is shown in Fig. 6. In general, increasing the HCl concentration increases the leaching efficiency, as indicated by an increase in the percentage of aluminum recovery as the number of H^+ ions available to attack the mineral lattice increases. Higher acid concentrations increase the concentration gradient between the particle surface and the solution, thereby enhancing mass transfer and accelerating the leaching reaction [48,49].

The kinetic parameter results in Table 2 show that with increasing HCl concentration from 1 M to 4 M, the effective diffusivity (De) in the Shrinking Core (SC) model increased from 0.00137 to 0.009308 cm²/s, indicating an increased rate of aluminum ion diffusion into the liquid phase. Meanwhile, the

reaction rate constant (k) remained relatively stable in the range of 3.6–6.85 cm/s, indicating that increasing concentration predominantly affected mass transport rather than intrinsic chemical reactions. In the Broken and Intact Cell (BIC) model, increasing HCl concentration also increased the De value (from 0.0769 to 0.0991 cm²/s) and the partition constant K (from 0.0109 to 0.0389 g/cm³), indicating increased ion mobility and solubility of aluminum compounds in solution. The SC model provided the best fit to the experimental data (lower RMSE values), indicating that the leaching process in this concentration range is more controlled by the chemical reaction rate at the solid–liquid interface. This result is in line with the findings of [50], where increasing HCl concentration accelerates the dissolution of aluminum from clay by reducing the diffusion resistance. However, at very high concentrations, increasing solution viscosity can reduce the effectiveness of mass transfer [51].

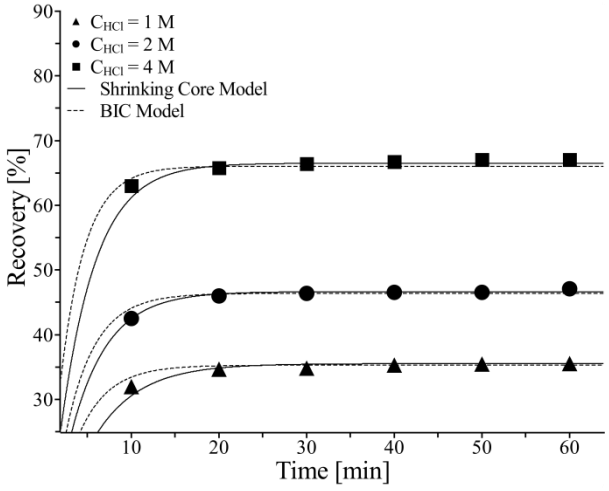

Fig. 6. Recovery of aluminum at particle size of 0.0074 cm and power of 100 W: effect of HCl concentration (1, 2, and 4 M) with comparison of two calculation models

3.8. Effect of temperature

The effect of temperature on aluminum leaching at a 4 M HCl concentration, a particle size of 0.0074 cm, and a microwave power of 100 W is shown in Fig. 7. In general, increasing the temperature from 20°C to 40°C significantly increases aluminum recovery. This phenomenon is caused by the increased kinetic energy of molecules and ionic diffusivity in the solution, which accelerates the mass transfer of H^+ ions to the particle surface and accelerates the aluminum dissolution process. Based on the calculations in Table 2, the effective diffusivity (De) value in the Shrinking Core (SC) model increases from 0.00494 cm²/s at 20°C to 0.01516 cm²/s at 40°C, indicating increased ion mobility and decreased diffusion resistance in the liquid film. However, the reaction rate constant (k) decreases from 10.5 cm/s to 6.2 cm/s. This indicates that at high temperatures, surface reactions begin to be limited by external mass transport rates, rather than intrinsic chemical reactions. In the Broken and Intact Cell (BIC) model, the De values and partition constant K increased significantly (from De = 0.0899 to 0.0991 cm²/s; from K = 0.0212 to 0.0439 g/cm³), indicating that high temperatures enhance the diffusion process between the broken cell and the solution. The SC model showed a better fit to the experimental data (lowest RMSE value), indicating that the leaching rate is still dominated by the reaction mechanism at the solid surface. These results are consistent with the literature [52], which reports that increasing temperature accelerates metal leaching kinetics by increasing activation energy and H^+ ion diffusion. However, at temperatures above 40 °C, excess thermal energy can cause a decrease in the degree of HCl ionization and partial solvent evaporation, thus reducing the overall leaching efficiency.

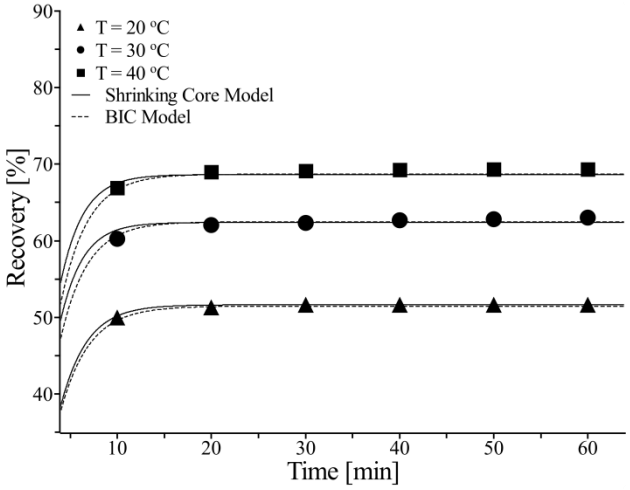

Fig. 7. Effect of temperature (20, 30, and 40 °C) on aluminum recovery with a comparison for the two calculation models at 4 M HCl concentration, 200 mesh particle size, and 100 Watt microwave power

The effective diffusivity (De) and reaction rate constant (k) values obtained from the Shrinking Core modeling in this study are pseudo-parameters resulting from numerical fitting, which represent the overall rate behavior of the heterogeneous leaching system. Given the scattering of the experimental data, especially in the later stages of the reaction when mass transfer barriers become dominant, the De and k values are not intended as absolute constants. Therefore, these parameters are used primarily to analyze trends relative to variations in microwave power and temperature, where consistent patterns of change provide relevant mechanistic information, although their numerical values are sensitive to data variations and model assumptions.

3.9. Effect of particle size

Fig. 8 shows the effect of particle size (0.0074 and 0.0149 cm) on aluminum recovery for both models. Increasing particle size negatively correlates with leach recovery. Smaller particles provide a larger specific surface area, shorten the diffusion distance of H^+ ions into the pores, and increase the number of damaged cells compared to intact cells. Consequently, diffusion resistance is reduced and aluminum dissolution occurs more rapidly. Conversely, with larger particles, most of the solute is trapped within intact cells, resulting in slower leaching and

limited to the particle surface.

The kinetic parameter results in Table 2 show that for the Shrinking Core (SC) model, 0.0074 cm particles have a De value of 0.01516 cm²/s and a k value of 6.20 cm/s, significantly higher than those for 0.0149 cm particles (De = 0.00358 cm²/s; k = 1.20 cm/s). This increase in De indicates that for smaller particles, the reaction rate is dominated by intraparticle diffusion. In the Broken and Intact Cell (BIC) model, the De value is also higher for small particles (0.09908 cm²/s) than for large particles (0.04808 cm²/s), indicating increased ion mobility due to the increased proportion of broken cells and the open diffusion pathways. A comparison of the two models shows that the SC model is more appropriate for large particle sizes (0.0149 cm) because the system is more controlled by the product layer and external diffusion, while the BIC model is more representative for small particles (0.0074 cm) because it can describe the simultaneous contributions of intact and broken cells. This finding supports the work of Zhang et al. [53], who reported that the smaller the particle size, the greater the contact area between HCl and the mineral surface, thus accelerating the dissolution rate. However, if the particle size is too fine, agglomeration can occur, reducing the effective contact area and inhibiting the diffusion of the solution into the particle pores.

Table 2 Values of coefficient parameters for SC and BIC models

Parameter		SC Model				BIC Model		
		D_e (cm²/s)	k (cm/s)	k_c (cm/s)	RMSE	D_e (cm²/s)	K (g/cm³)	RMSE
Microwave power P (watt)	80	0.002708	1.28	2.756	0.1736	0.0508	0.0102	0.22850
	100	0.001390	3.58	0.990	0.3480	0.08039	0.0106	0.22830
HCl concentration C_{HCl} (M)	1	0.001370	6.85	0.929	0.1727	0.0769	0.0109	0.19726
	2	0.003369	3.80	2.030	0.0277	0.0804	0.0173	0.22229
	4	0.009308	3.60	4.119	0.2937	0.0991	0.0389	0.26844
Temperature T (°C)	20	0.004940	10.5	2.490	0.0088	0.0899	0.0212	0.02477
	30	0.009829	8.02	4.320	0.1492	0.0984	0.0333	0.05371
	40	0.015160	6.20	6.289	0.1400	0.0991	0.0439	0.10005
Particle size dp (cm)	0.0074	0.015160	6.20	6.289	0.1400	0.09908	0.0439	0.10005
	0.0149	0.003580	1.20	0.909	0.0074	0.04808	0.0269	0.02961

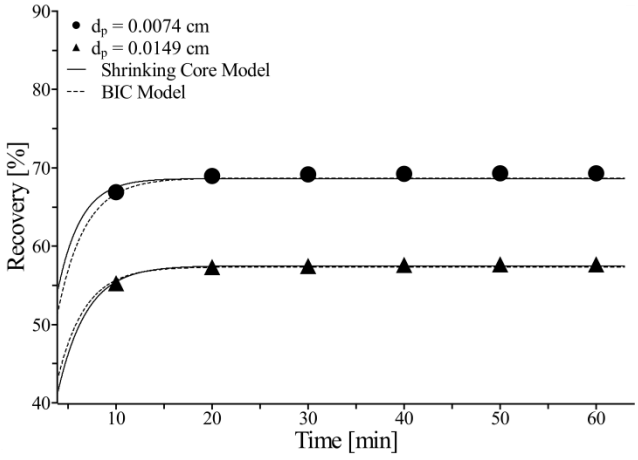

Fig. 8. Recovery of aluminum at particle sizes of 0.0074 and 0.0149 cm: comparison of two calculation models at 4 M HCl, 40 °C, and 100 W

3.10. Process performance index

The Process Performance Index (PPI) indicator is used to evaluate the overall effectiveness of the leaching process by combining two main aspects of the process: the amount of alumina successfully extracted and operational inputs in the form of energy and HCl make-up requirements. The PPI is calculated as the ratio between the process output value (R) and the total operating cost (C_{tot}). Thus, the PPI serves as a synthetic measure that assesses the balance between technical efficiency and process input intensity, without being oriented towards financial returns. The variable that most influences the high PPI value is the alumina extraction efficiency (η).

Table 3 shows the evaluation of leaching process using Process Performance Index (PPI). The greater the recovery, the greater the output value (R), while the energy and HCl make-up costs are relatively very small and almost constant between conditions. Consequently, the condition with the highest recovery automatically has the highest PPI value. This is seen in the leaching condition using 4 M HCl at 40 °C, which provides the highest recovery (68.3%) and produces the largest PPI value across all scenarios. However, the PPI value is not solely determined by extraction efficiency. In scenario No. 3 (2 M, 40 °C), the PPI value (542.6) is higher than scenario No. 5 (4 M, 20 °C) which has a higher recovery (51.4% vs. 46.1%).

This indicates that a lower HCl concentration can improve process effectiveness, as the need for make-up HCl is smaller, resulting in a decrease in total operational costs (C_{tot}). Thus, the PPI value can increase even if recovery does not reach the maximum value, as long as the process input especially HCl consumption is more efficient. This finding indicates that PPI optimization requires a balance between high recovery and minimizing reagent consumption, rather than simply maximizing one or the other. This finding is in line with previous literature [54,55]. Those showed that increasing acid concentration and temperature directly increased the rate and efficiency of alumina leaching. Meanwhile, the use of microwaves in the leaching process has been shown to accelerate mineral disintegration and enhance ion diffusion, thereby increasing extraction without significantly increasing energy consumption [56,57]. In this study, the very low electrical energy but high recovery contributed significantly to the superior PPI value.

Compared with conventional methods, microwave-assisted leaching has proven to be more efficient due to its ability to provide volumetric heating and accelerate the reaction. Compared with the Bayer process, this method is also more suitable for non-bauxite materials such as peat or clay, which are generally not economically processable with the Bayer process due to their high silica content. Several studies, including those by Kim et al. [57], confirm that microwave pretreatment can increase aluminum solubility in difficult-to-process materials. Overall, based on PPI values, leaching conditions of 4 M and 40 °C are the most optimal configuration in the HCl regeneration system and low energy consumption. This confirms that alumina recovery is the dominant factor in determining process effectiveness, and the microwave method offers significant technical advantages over conventional leaching and the Bayer process for non-bauxite materials.

Table 3 Evaluation of leaching process performance based on extraction efficiency and process performance index

Power (Watt)	HCl	Temperature (°C)	Particle size (cm)	Al recovery (%)	Revenue ($)	Energy Cost ($)	HCl Cost ($)	Total Cost ($)	PPI
80	1 M	40	0.0074	33.4	0.747	0.00133	0.00012	0.00145	515.2
100	1 M	40	0.0074	35.3	0.79	0.00167	0.00012	0.00179	441.3
100	2 M	40	0.0074	46.1	1.031	0.00167	0.00023	0.0019	542.6
100	4 M	40	0.0074	68.3	1.528	0.00167	0.00047	0.00214	714.0
100	4 M	20	0.0074	51.4	1.15	0.00167	0.00047	0.00214	537.4
100	4 M	30	0.0074	62.6	1.401	0.00167	0.00047	0.00214	654.7
100	4 M	40	0.0149	56.8	1.271	0.00167	0.00047	0.00214	593.9

4. Conclusions

Aluminum in peat clay was leached using HCl as a solvent to determine the influence of HCl concentration, microwave power, temperature, pressure, and particle size on the aluminum recovery. Aluminum recovery increase with increasing in particle size, and also increase with increasing HCl concentration, microwave power, and temperature. Furthermore, the experimental data well fitted the models of SC and BIC at microwave-assisted leaching process. From the comparison between experimental data and models, the SC model can illustrate experimental data well for all extraction conditions except at higher temperature and particle size, while the BIC model can only describe well for lower temperature and particle size compare with SC model. The kinetic parameters obtained for the SC model are De = 0.0049 cm²/s, k = 10.5 cm/s, and kc = 2.49 cm/s, while for the BIC model are De = 0.04808 cm²/s and K = 0.02689 g/cm³. These values indicate that the diffusion of H^+ ions and the protonation reaction on the Al–O–Si surface are the main controlling steps in microwave-assisted aluminum leaching. Furthermore, evaluation using the Process Performance Index (PIK) shows that leaching effectiveness is not only determined by high aluminum recovery, but also by the efficiency of reagent and energy consumption. Leaching conditions of 4 M HCl at 40 °C provide the highest PKI because they produce the largest aluminum recovery, but conditions with lower HCl concentrations can also provide competitive PKI values when the need for HCl make-up is minimal. This confirms that optimization of the leaching process requires a balance between high aluminum recovery and efficient reagent use, resulting in more effective and sustainable process performance. Thus, this study confirms that the integration of microwave energy with an HCl acid system can improve the kinetics of aluminum leaching from non-bauxite materials such as peat loam, while expanding the application of the SC and BIC models to aluminosilicate-rich materials.

Nomenclature

A	particle surface area (cm^2)
A_i	intact cell surface area (cm^2)
B	ratio of solvents and solids (cm^3/g)
c_{Al}	concentration of solute in the solvent (g/cm^3)
C_{Al}	solvent concentration (g/L)
$C_{A(R)}$	aluminum leaching concentration (g/L)
D_e	effective diffusivity (cm^2/s)
E	mean relative deviation *modulus* (-)
f	volumetric fraction of surface area (-)
k	reaction rate constants (cm/s)
k_c	liquid phase mass transfer coefficient (cm/s)

k_p solid phase mass transfer coefficient (cm/s)
K partition constant (g/cm^3)
K_1 first partition constant (g/cm^3)
K_2 second partition constant (g/cm^3)
m solid mass (g)
M mass transfer rate (g/s)
N number of experimental points (-)
$\overline{q}$ average value of q (g/L)
q_i concentration of solid phase in intact cells (g/L)
q_u initial solid phase concentration (g/L)
r radial coordinates
r' correlation coefficient (-)
r_c the critical radius of the core (cm)
R particle radius (cm)
R_i cell intact radius (cm)
$RMSE$ root mean square error
t time (s)

Greek letters

π circle ratio (3,14159)
ε empty fraction (-)
ρ_p solid density (g/cm^3)

Acknowledgment

The author expresses his appreciation and gratitude to the Department of Chemical Engineering, Lambung Mangkurat University for the support and facilities provided during the research, especially in the Industrial Water and Wastewater Treatment Laboratory and the Simulation and Modeling Laboratory. This experimental and modeling studies was supported financially by the Directorate General of Higher Education, Ministry of Higher Education, Science, and Technology of the Republic of Indonesia with contract 075/C3/DT.05.00/PL/2025.

Reference

1. Z. Ma, Q. Zhong, A. Calzadilla, M. Winning, The dynamic global aluminium use across production systems to consumption systems, Ecological Economics 239 (2026) 108770.
2. D. Brough, H. Jouhara, The aluminium industry: A review on state-of-the-art technologies, environmental impacts and possibilities for waste heat recovery, International Journal of Thermofluids 1–2 (2020) 100007.
3. A. Shilla, G. Mwandila, Review of methods for alumina recovery from mudstone and coal fly ash, Heliyon 10 (2024) e34812.
4. A. Mirwan, S. Susianto, A. Altway, R. Handogo, Kinetic model for identifying the rate controlling step of the aluminum leaching from peat clay, Jurnal Teknologi (Sciences & Engineering) 80 (2018).
5. J. Xu, P.J. Morris, J. Liu, J. Holden, PEATMAP: Refining estimates of global peatland distribution based on a meta-analysis, CATENA 160 (2018) 134–140.
6. G.C. Dargie, S.L. Lewis, I.T. Lawson, E.T.A. Mitchard, S.E. Page, Y.E. Bocko, S.A. Ifo, Age, extent and carbon storage of the central Congo Basin peatland complex, Nature 542 (2017) 86–90.
7. S.E. Page, J.O. Rieley, C.J. Banks, Global and regional importance of the tropical peatland carbon pool, Global Change Biology 17 (2011) 798–818.
8. E.P. Meshcheryakov, S.I. Reshetnikov, M.P. Sandu, A.S. Knyazev, I.A. Kurzina, Efficient Adsorbent-Desiccant Based on Aluminium Oxide, Applied Sciences 11 (2021) 2457.
9. F.M. Kaußen, B. Friedrich, Methods for Alkaline Recovery of Aluminum from Bauxite Residue, J. Sustain. Metall. 2 (2016) 353–364.
10. Z. Yuan, H. Liu, W. Fen Yong, Q. She, J. Esteban, Status and advances of deep eutectic solvents for metal separation and recovery, Green Chemistry 24 (2022) 1895–1929.
11. T. Punt, G. Akdogan, S. Bradshaw, P. van Wyk, Development of a novel solvent extraction process using citric acid for lithium-ion battery recycling, Minerals Engineering 173 (2021) 107204.
12. Y. Mubula, M. Yu, D. Yang, H. Niu, H. Gu, T. Qiu, G. Mei, Microwave-assisted atmospheric alkaline leaching process and leaching kinetics of rare earth melt electrolysis slag, Heliyon 10 (2024) e32278.
13. S. Chae, K. Yoo, C.B. Tabelin, R.D. Alorro, Hydrochloric Acid Leaching Behaviors of Copper and Antimony in Speiss Obtained from Top Submerged Lance Furnace, Metals 10 (2020) 1393.
14. A. Mirwan, S. Susianto, A. Altway, R. Handogo, Temperature-dependent kinetics of aluminum leaching from peat clay, Malaysian Journal of Fundamental and Applied Sciences 16 (2020) 248–251.
15. J. Wang, Y. Zhang, J. Huang, T. Liu, Kinetic and Mechanism Study of Vanadium Acid Leaching from Black Shale Using Microwave Heating Method, JOM 70 (2018) 1031–1036.
16. Z. Ma, Y. Liu, J. Zhou, M. Liu, Z. Liu, Recovery of vanadium and molybdenum from spent petrochemical catalyst by microwave-assisted leaching, Int J Miner Metall Mater 26 (2019) 33–40.
17. Y. Chen, J. Zhou, L. Zhang, J. Peng, S. Li, S. Yin, K. Yang, Y. Lin, Microwave-assisted and regular leaching of germanium from the germanium-rich lignite ash, Green Processing and Synthesis 7 (2018)
18. V. Lovrić, P. Putnik, D.B. Kovačević, M. Jukić, V. Dragović-Uzelac, Effect of Microwave-Assisted Extraction on the Phenolic Compounds and Antioxidant Capacity of Blackthorn Flowers, Food Technol Biotechnol 55 (2017) 243–250.
19. A. Kumar, M. Gayoor Khan, The Scenario of Pharmaceuticals and Development of Microwave Assisted Extraction Techniques, (2019).
20. R.V. Kapoore, T.O. Butler, J. Pandhal, S. Vaidyanathan, Microwave-Assisted Extraction for Microalgae: From Biofuels to Biorefinery, Biology 7 (2018) 18.
21. D.R. Wicakso, A. Mirwan, E. Agustin, N.F. Nopembriani, I. Firdaus, M. Fadillah, Potential of silica from water treatment sludge modified with chitosan for Pb(II) and color adsorption in sasirangan waste solution, Communications in Science and Technology 7 (2022) 188–193.
22. L. Guo, J. Lan, Y. Du, T.C. Zhang, D. Du, Microwave-enhanced selective leaching of arsenic from copper smelting flue dusts, Journal of Hazardous Materials 386 (2020) 121964.
23. O.R. Alara, N.H. Abdurahman, Microwave-assisted extraction of phenolics from *Hibiscus sabdariffa* calyces: Kinetic modelling and process intensification, Industrial Crops and Products 137 (2019) 528–535.
24. H. Sovová, Broken-and-intact cell model for supercritical fluid extraction: Its origin and limits, The Journal of Supercritical Fluids 129 (2017) 3–8.
25. M. Bonfigli, E. Godoy, M.A. Reinheimer, N.J. Scenna, Comparison between conventional and ultrasound-assisted techniques for extraction of anthocyanins from grape pomace. Experimental results and mathematical modeling, Journal of Food Engineering 207 (2017) 56–72.
26. A. Bucić-Kojić, H. Sovová, M. Planinić, S. Tomas, Temperature-dependent kinetics of grape seed phenolic compounds extraction:

Experiment and model, Food Chemistry 136 (2013) 1136–1140.
27. N.B. Singh, Clays and Clay Minerals in the Construction Industry, Minerals 12 (2022) 301.
28. A. Mirwan, M.D. Putra, J.-C. Liu, Susianto, A. Altway, R. Handogo, Aluminum leaching from water treatment sludge using hydrochloric acid and kinetic study, Environ Sci Pollut Res 27 (2020) 25553–25562.
29. H. Hong, S. Chen, Q. Fang, T.J. Algeo, L. Zhao, Adsorption of organic matter on clay minerals in the Dajiuhu peat soil chronosequence, South China, Applied Clay Science 178 (2019) 105125.
30. J. Cao, S. Huang, W. Liu, C. Kong, Y. Gao, F. Liu, Study on Simulation Test of Peat Soil Environment in Dianchi Lake, Advances in Civil Engineering (n.d.).
31. J.A. Rahman, A.M.A. Napia, M.A.A. Nazri, R.M.S.R. Mohamed, A.S. Al-Geethi, A Study on Factors Affecting Strength of Solidified Peat through XRD and FESEM Analysis, IOP Conf. Ser.: Earth Environ. Sci. 140 (2018) 012059.
32. E.D. Ningsih, R. Putra, C.D. La Maisonneuve, M. Phua, S. Eisele, F. Forni, J. Oalmann, H. Rifai, Identification of magnetic mineral forming elements in peatland Alahan Panjang West Sumatra Indonesia, section DD REP B 693 using X-Ray Fluorescence, J. Phys.: Conf. Ser. 1481 (2020) 012018.
33. M. Al-Harahsheh, S.W. Kingman, Microwave-assisted leaching—a review, Hydrometallurgy 73 (2004) 189–203.
34. G. Gluth, C. Grengg, N. Ukrainczyk, F. Mittermayr, M. Dietzel, Acid resistance of alkali-activated materials: recent advances and research needs, RILEM Technical Letters 7 (2022) 58–67.
35. M. Saldaña, E. Gálvez, P. Robles, J. Castillo, N. Toro, Copper Mineral Leaching Mathematical Models—A Review, Materials (Basel) 15 (2022) 1757.
36. J. Zheng, Z. Zheng, L. Li, X. Li, W. Liu, Z. Lin, Acid-leaching mechanism of electroplating sludge: based on a comprehensive analysis of heavy-metal occurrence and the dynamic evolution of coexisting mineral phases, Environ Sci Pollut Res Int 30 (2023) 113600–113608.
37. B. Hu, C. Zhang, X. Zhang, The Effects of Hydrochloric Acid Pretreatment on Different Types of Clay Minerals, Minerals 12 (2022) 1167.
38. V.I. Pak, S.S. Kirov, A.Y. Nalivaiko, D.Y. Ozherelkov, A.A. Gromov, Obtaining Alumina from Kaolin Clay via Aluminum Chloride, Materials 12 (2019) 3938.
39. J. Chen, X. Li, L. Gao, S. Guo, F. He, Microwave Treatment of Minerals and Ores: Heating Behaviors, Applications, and Future Directions, Minerals 14 (2024) 219.
40. V.J. Inglezakis, M. Balsamo, F. Montagnaro, Liquid–Solid Mass Transfer in Adsorption Systems—An Overlooked Resistance?, Industrial & Engineering Chemistry Research (2020).
41. R. Shiba, Md.A. Uddin, Y. Kato, S. Kitamura, Solid/liquid Mass Transfer Correlated to Mixing Pattern in a Mechanically-stirred Vessel, ISIJ International 54 (2014) 2754–2760.
42. S. Cheng, C. Zhong, T.A.G. Langrish, Y. Sun, Z. Zhou, Z. Lei, The relative importance of internal and external physical resistances to mass transfer for caffeine release from apple pectin tablets, Curr Res Food Sci 5 (2022) 634–641.
43. F.S. Mohammad, E.A.H. Al Zubaidy, G. Bassioni, Effect of Aluminum Leaching Process of Cooking Wares on Food, International Journal of Electrochemical Science 6 (2011) 222–230.
44. D. Yang, M. Yu, Y. Zhao, M. Cheng, G. Mei, Leaching Kinetics of Y and Eu from Waste Phosphors under Microwave Irradiation, Processes 11 (2023) 1939.
45. X. Bu, Z. Tong, M. Bilal, X. Ren, M. Ni, C. Ni, G. Xie, Effect of ultrasound power on HCl leaching kinetics of impurity removal of aphanitic graphite, Ultrason Sonochem 95 (2023) 106415.
46. A. Zhu, X. Bian, W. Han, Y. Wen, K. Ye, G. Wang, J. Yan, D. Cao, K. Zhu, S. Wang, Microwave-ultra-fast recovery of valuable metals from spent lithium-ion batteries by deep eutectic solvents, Waste Management 156 (2023) 139–147.
47. J. Chen, X. Li, L. Gao, S. Guo, F. He, Microwave Treatment of Minerals and Ores: Heating Behaviors, Applications, and Future Directions, Minerals 14 (2024) 219.
48. S. Chae, K. Yoo, C.B. Tabelin, R.D. Alorro, Hydrochloric Acid Leaching Behaviors of Copper and Antimony in Speiss Obtained from Top Submerged Lance Furnace, Metals 10 (2020) 1393.
49. R. Chi, J. Tian, G. Zhu, Y. Wu, S. Li, C. Wang, Z.A. Zhou, Kinetics of Rare Earth Leaching from a Mangnese-Removed Weathered Rare-Earth Mud in Hydrochloric Acid Solutions, Separation Science and Technology 41 (2006) 1099–1113.
50. X. Lv, Q. Wu, X. Huang, L. ling Wu, L. Hu, P. Fei, T. ming Liu, Q. Yu, Effect of Microwave Pretreatment on the Leaching and Enrichment Effect of Copper in Waste Printed Circuit Boards, ACS Omega 8 (2023) 2575–2585.
51. Y. Mubula, M. Yu, D. Yang, H. Niu, H. Gu, T. Qiu, G. Mei, Microwave-assisted atmospheric alkaline leaching process and leaching kinetics of rare earth melt electrolysis slag, Heliyon 10 (2024) e32278.
52. M. Al-Harahsheh, S.W. Kingman, Microwave-assisted leaching—a review, Hydrometallurgy 73 (2004) 189–203.
53. Y. Li, S. Zhu, L. Wang, Purification of natural graphite by microwave assisted acid leaching, Carbon 55 (2013) 377–378.
54. I.A. Nnanwube, O.D. Onukwuli, Characterization and kinetics of alumina leaching from calcined Akpugo kaolinite for potential aluminum recovery, South African Journal of Chemical Engineering 43 (2023) 24–37.
55. M.A. Tantawy, A.A. Alomari, Extraction of Alumina from Nawan Kaolin by Acid Leaching, Oriental Journal of Chemistry 35 (2019) 1013–1021.
56. J.A. Cecilia, L. Pardo, M. Pozo, E. Bellido, F. Franco, Microwave-Assisted Acid Activation of Clays Composed of 2:1 Clay Minerals: A Comparative Study, Minerals 8 (2018) 376.
57. Z.-Y. Zhang, X.-C. Qiao, J.-G. Yu, Aluminum release from microwave-assisted reaction of coal fly ash with calcium carbonate, Fuel Processing Technology 134 (2015) 303–309.
58. J.-S. Kim, N.-C. Choi, H.Y. Jo, Selective Leaching Trace Elements from Bauxite Residue (Red Mud) without and with Adding Solid NH4Cl Using Microwave Heating, Metals 11 (2021) 1281.